Environmental Pollution 259 (2020) 113954

Contents lists available at ScienceDirect

Environmental Pollution

journal homepage: www.elsevier.com/locate/envpol

Consistent trace element distribution and mercury isotopic signature between a shallow buried volcanic-hosted epithermal gold deposit and its weathered horizon☆

Runsheng Yin [a, *], Xin Pan [a, b], Changzhou Deng [a], Guangyi Sun [c], Sae Yun Kwon [d], Ryan F. Lepak [e], James P. Hurley [e]

[a] State Key Laboratory of Ore Deposit Geochemistry, Institute of Geochemistry, Chinese Academy of Sciences, Guiyang, 550081, China
[b] University of Chinese Academy of Sciences, Beijing, 100049, China
[c] State Key Laboratory of Environmental Geochemistry, Institute of Geochemistry, Chinese Academy of Sciences, Guiyang, 550081, China
[d] Division of Environmental Science & Engineering, Pohang University of Science and Technology, 77 Cheongam-Ro, Nam Gu, Pohang, 37673 South Korea
[e] Environmental Chemistry and Technology Program, University of Wisconsin-Madison, Madison, WI, 53706, USA

ARTICLE INFO

Article history:
Received 27 October 2019
Received in revised form
30 December 2019
Accepted 8 January 2020
Available online 9 January 2020

Keywords:
Trace elements
Mercury isotope
Weathered horizon
Geochemical prospecting
Hydrothermal gold deposit

ABSTRACT

Trace elements and Hg isotopic composition were investigated in mineralized rocks, barren rocks, and mineral soils in the Xianfeng prospect, a shallow buried epithermal gold deposit in northeastern China, to understand whether this deposit has left a diagnostic geochemical fingerprint to its weathered horizon. All the rocks and soils display congruent patterns for immobile elements (large ion lithophile elements, high field strength elements, and rare earth elements), which reflect the subduction-related tectonic setting. Both mineralized rocks and soils showed common enrichment of elemental suite As−Ag−Sb−Hg, suggesting that the Xianfeng gold deposit has released these elements into its weathered horizon. Similar mercury isotopic composition was observed between mineralized rocks (δ^{202}Hg: −0.21 ± 0.70‰; Δ^{199}Hg: −0.02 ± 0.12‰; 2SD) and barren rocks (δ^{202}Hg: −0.46 ± 0.48‰; Δ^{199}Hg: 0.00 ± 0.10‰; 2SD), suggesting that mercury in the Xianfeng deposit is mainly derived from the magmatic rocks. Mineralized soils (δ^{202}Hg: −0.44 ± 0.60‰; −0.03 ± 0.14‰; 2SD) and barren soils (δ^{202}Hg: −0.54 ± 0.68‰; Δ^{199}Hg: −0.05 ± 0.14‰; 2SD) displayed congruent Hg isotopic signals to the underlying rocks, suggesting limited Hg isotope fractionation during the release of Hg from ore deposit to soils via weathering. This study reveals evidence of a simple and direct geochemical link between this shallow buried hydrothermal deposit and its weathered horizon, and highlights that the weathering of shallow-buried hydrothermal gold deposits can release a substantial amount of heavy metals (e.g. Hg, As and Sb) to surface soil.

1. Introduction

Due to its chalcophilic nature, mercury (Hg) is found in abundance in sulfide minerals in hydrothermal deposits, making them the most important pools of Hg in the Earth's crust (Rytuba, 2003). Hydrothermal gold (Au) deposits have common enrichments of Hg and other chalcophile elements such as arsenic (As)-antimony (Sb) (Hedenquist et al., 2000; Saunders et al., 2014). These metals are also known as heavy metals, which are of great environmental concern. The weathering of shallow buried gold deposits may leave high anomalies of Au−As−Sb−Hg in the weathered soil horizon, although these anomalies may be distorted by leaching, seepage, and solid physical processes. Meanwhile, the weathering of shallow buried gold deposits represents as an important source of heavy metals to the weathered soil horizon. Systematic analysis of the Au−As−Sb−Hg anomalies in the weathered horizon, where the soil is residual and mineralization is not covered by younger rocks or transported overburden, represents a straightforward method of prospecting buried orebodies (Bradshaw et al., 1979; Freyssinet et al., 1997).

The measurements of mercury isotopes and their geochemistry have become a new discipline for understanding the sources and

☆ This paper has been recommended for acceptance by Dr. Yong Sik Ok.

* Corresponding author.
E-mail address: yinrunsheng@mail.gyig.ac.cn (R. Yin).

https://doi.org/10.1016/j.envpol.2020.113954
0269-7491/

fates of Hg in hydrothermal ore deposits (Hintelmann and Lu, 2003; Smith et al., 2005; Smith et al., 2008; Sonke et al., 2010; Yin et al., 2016a; Tang et al., 2017; Xu et al., 2017). Natural stable isotopes of mercury (^{196}Hg, ^{198}Hg, ^{199}Hg, ^{200}Hg, ^{201}Hg, ^{202}Hg, and ^{204}Hg) can undergo both mass-dependent fractionation (MDF, defined as δ^{202}Hg) and mass-independent fractionation (MIF, defined as Δ^{199}Hg). The MDF of Hg isotopes is ubiquitous and occurs during a variety of biogeochemical processes in the mercury cycle (Bergquist and Blum, 2009). The MIF of Hg isotopes is widely observed in Earth's surface pools (e.g. soil, sediment, water, atmosphere, and biota), and is mainly generated during Hg photochemical reactions in the aquatic environment (Blum et al., 2014; Sonke, 2011). This makes Hg-MIF a powerful tracer for distinguishing between syngenetic and epigenetic Hg in hydrothermal deposits (Xu et al., 2017; Yin et al., 2019). Syngenetic Hg in magmatic/mantle materials is characterized by the absence of MIF (Δ^{199}Hg ~ 0), and epigenetic Hg in sedimentary rocks has significant MIF signals (Δ^{199}Hg $\neq$ 0) (Yin et al. (2016a) and references therein).

In northeastern (NE) China, a large number of hydrothermal gold deposits have been discovered in the last decades (Zhou et al., 2002; Han et al., 2013; Zhai et al., 2015). Most of these deposits are associated with extensive forest cover and poor rock exposure, and exploratory trenching has been employed as a conventional method for prospection. With the increased preservation of forests and ecosystems in recent years, extensive exploratory trenches have been forbidden by the Chinese Forestry Administration. The application of soil sampling for geochemical exploration, which has low environmental and practical costs, should, therefore, be considered. To date, however, it is still unclear whether the isotopic composition of Hg in weathered horizon can be used for prospecting shallowly buried orebodies, because soil not only receives Hg from the weathered rocks but also via atmospheric deposition, and the two Hg sources have distinct isotope signatures (Zhang et al., 2013).

Through a recent project, we systemically collected mineralized rocks, barren rocks, and their overlying mineral soils from the Xianfeng gold prospect, a shallow buried epithermal gold in northeastern China. In our recent study about the Xianfeng deposit (Yin et al., 2019), we observed anomalously high Hg levels in mineralized rocks (geometric mean: 0.68 μg g^{-1}; n = 33) compared to barren rocks (geometric mean: 0.02 μg g^{-1}; n = 25). The isotopic compositions of Hg in rock samples were also studied, which displayed consistent Hg isotopic signals between mineralized rocks (δ^{202}Hg: −0.23 ± 0.72‰; Δ^{199}Hg: −0.02 ± 0.12‰; 2SD, n = 33) and barren rocks (δ^{202}Hg: −0.45 ± 0.44‰; Δ^{199}Hg: −0.01 ± 0.12‰; 2SD, n = 13). The absence of Hg-MIF in these rocks suggested that Hg in the Xianfeng gold deposit is of syngenetic origin (Yin et al., 2019). We further hypothesized that hydrothermal deposits may leave a diagnostic elemental and Hg isotopic signal in their weathered horizon. In this study, we conducted analysis of the concentrations and isotopic compositions of Hg in soil samples. The trace elements in both rock and soil samples were also measured. The aims of this study are to test: (1) whether the Xianfeng deposit left a diagnostic elemental distribution pattern in the weathered horizon, (2) whether the weathering of shallow buried hydrothermal deposits can release heavy metals to surface soil, and (3) whether Hg isotope compositions are similar between orebodies and weathered horizon in the Xianfeng deposit.

2. Sampling and analytical methods

2.1. Study area

The Xianfeng gold prospect located in NE China is geologically situated in the eastern section of the Central Asian Orogenic Belt (CAOB), which is a giant accretionary orogen bounded by the Siberian, Tarim and North China cratons (Fig. 1A). Voluminous granitoids and other magmatic rocks were emplaced during the Paleozoic and Mesozoic eras in NE China (Zhai et al., 2015) and formed an essential crustal component in the studied area (Fig. 1B). The studied area is characterized by widespread occurrences of hydrothermal gold deposits (Li, 2011), which show a consistent spatiotemporal association with the Mesozoic magmatic rocks (Fig. 1B).

The geology of the Xianfeng deposit has been described in our recent study (Yin et al., 2019). Briefly, it is a ~117 Ma old volcanic-hosted epithermal gold system. The gold resource in this deposit remains confidential. As shown in Fig. 2, igneous rocks including 128 Ma granodiorite and 106 Ma diorite porphyry are distributed in the studied area. This deposit consists of brecciated, veined and lenticular orebodies, which are hosted in the Early Cretaceous hydrothermal breccias in the NW part of the deposit (Fig. 2A and B). Sporadic anomalies (weak gold mineralization) also occur in the rhyolitic tuffs at the SE part of the deposit. Pyrite, hematite, minor chalcopyrite, and magnetite are the ore minerals. Pyrite is the most abundant sulfide and the main gold-bearing mineral. Native gold (>1 μm) occurs in pyrite or along quartz crystal boundaries. Quartz, chalcedony, adularia, and calcite are the main gangue minerals. The major hydrothermal alteration types include silicification, sericitization, carbonatization, and kaolinization (Yin et al., 2019).

2.2. Sampling

In our project, a total of 58 sites along a prospecting trench in the Xianfeng prospect were chosen for sampling in September 2016 (Fig. 2B). At 43 sites, fresh rock and paired soil samples were collected. At the remaining sites (15 sites), only rock samples were collected due to the lack of weathered horizon. The soil profiles are generally consisted of A horizon (a surface mineral horizon showing coloration due to organic matter accumulation), B horizon (a subsurface horizon showing depletion of organic matter) and C horizon (a subsurface layer of soil with parent materials), with thickness of 0–10 cm, 10–30 cm, 10–20 cm, respectively. Soil samples (0.5–1 kg for each sample) were only collected from B horizon, because A horizon likely receives Hg via atmospheric deposition as reported from previous studies (Jiskra et al., 2017; Biswas et al., 2008; Kwon et al., 2015), and C horizon contains large rock fragments. Fresh rock samples (~1 kg for each sample) were collected underlying C horizon. All soil and rock samples were stored in sealed polyethylene bags to avoid cross-contamination. In the laboratory, the soil samples were air-dried at room temperature, ground, homogenized, and sieved to sub-minus 150 μm mesh, prior to chemical analysis. Details about the pretreatment of rock samples, Hg concentrations, and isotopic compositions have been reported in our recent study (Yin et al., 2019).

2.3. Analytical methods

Bulk gold concentrations of soil and rock samples were measured by ALS-Chemex Co. Ltd, Guangzhou, China, using the fire assay technique with gravimetric finish (Code Au-GRA22; detection limit: 0.05 μg g^{-1} Au). Trace elements in soil and rock samples were measured at the Institute of Geochemistry, Chinese Academy of Sciences (IGCAS), using a PerkinElmer Sciex ELAN 6000 inductively-coupled plasma mass spectrometer (Tan et al., 2015). This method provides data for large ion lithophile elements (LILE: Rb, Cs, Sr, Ba, and U), high field strength elements (HFSE: Nb, Ta, Zr, Hf, Th and Ti), rare earth elements (REE: La, Ce, Pr, Nd, Sm, Eu, Gd, Tb, Dy, Ho, Er, Tm, Yb and Lu) and chalcophile elements (Cu, Zn, Ga, Ge, As, Ag, Cd, In, Sn, Sb, Tl and Pb). The measurement accuracy of

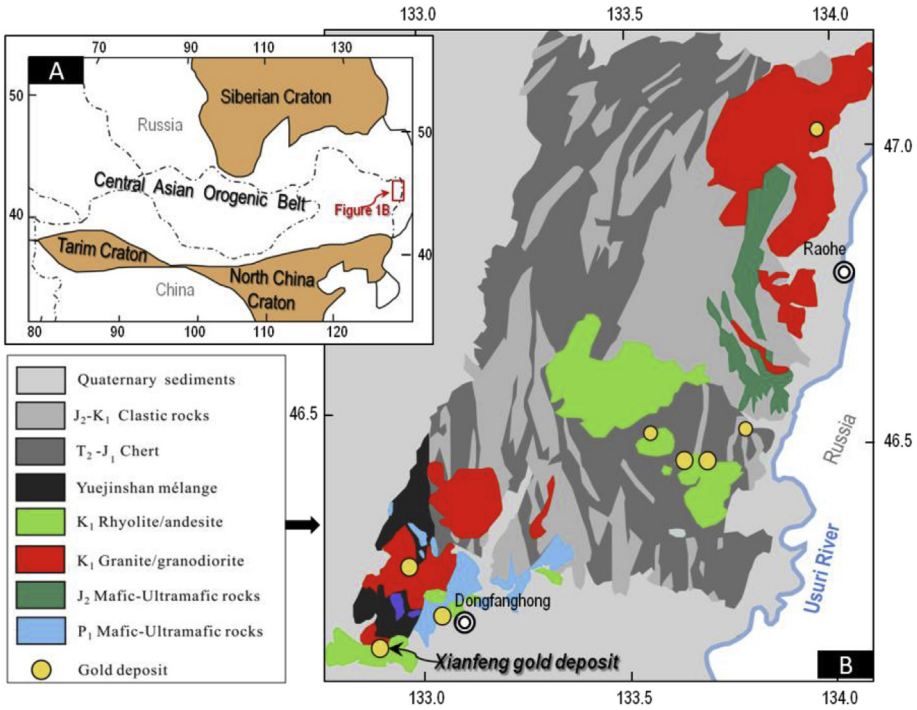

Fig. 1. **A** Tectonic subdivisions of NE China (modified after Wu et al. (2007)); **B** A simplified geological map of the studied area (modified after Sun et al. (2015) and Li (2011)).

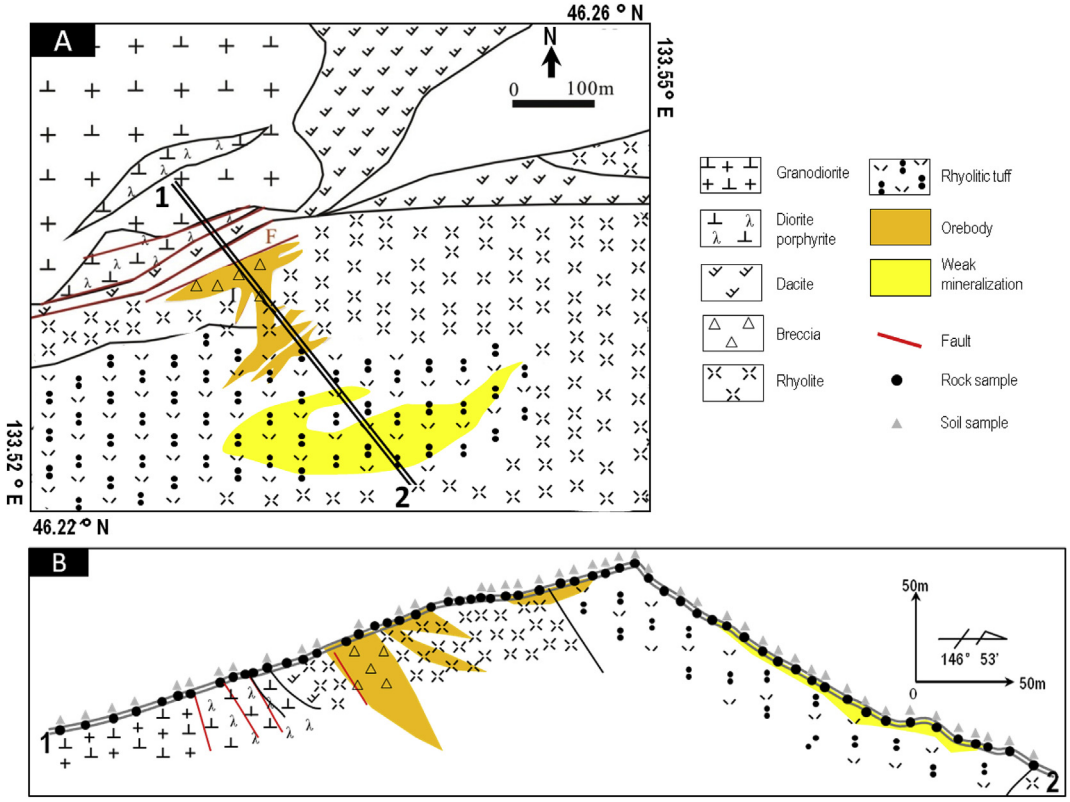

Fig. 2. **A** Simplified geological map of the Xianfeng gold deposit (modified after Wang (2015)); **B** Geological cross-section of the Xianfeng Au deposit (modified after Li (2011)). (For interpretation of the references to color in this figure legend, the reader is referred to the Web version of this article.)

all elements using the standard reference material GSR1 (granite) was within ±10% (n = 3) of the reported values.

Bulk Hg concentrations of soil samples were determined using a Lumex RA 915 + Hg analyzer (detection limit: 0.5 ng g^{-1} Hg) at IGCAS, following the method by Sholupov et al. (2004). Recoveries of Hg in standard reference materials NIST SRM 2711 and MESS-1

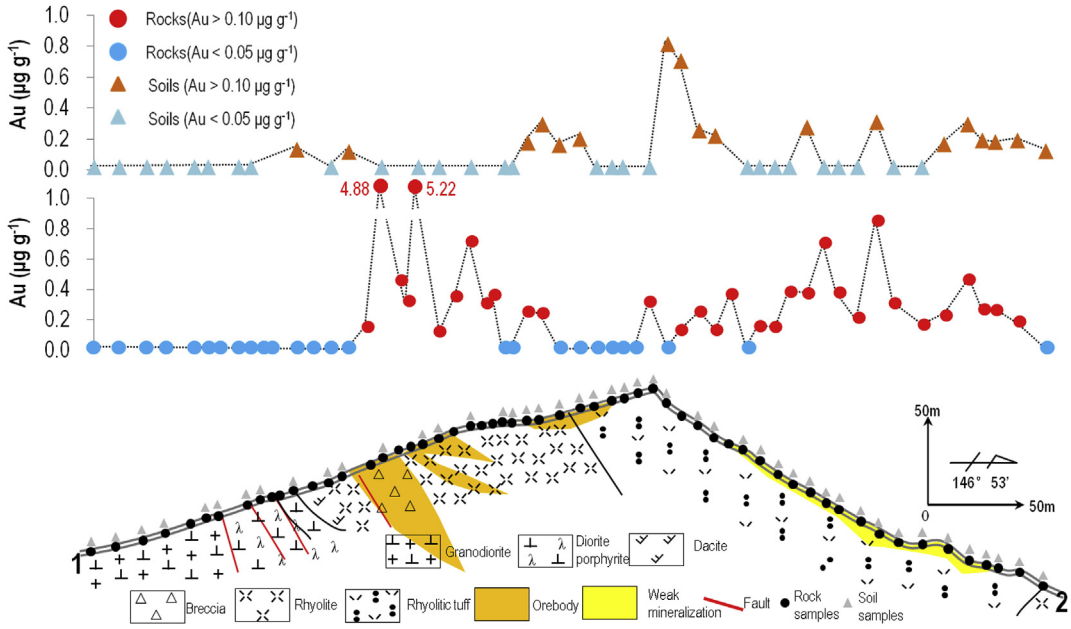

Fig. 3. Gold concentrations in rocks and soils from the Xianfeng gold deposit. (For interpretation of the references to color in this figure legend, the reader is referred to the Web version of this article.)

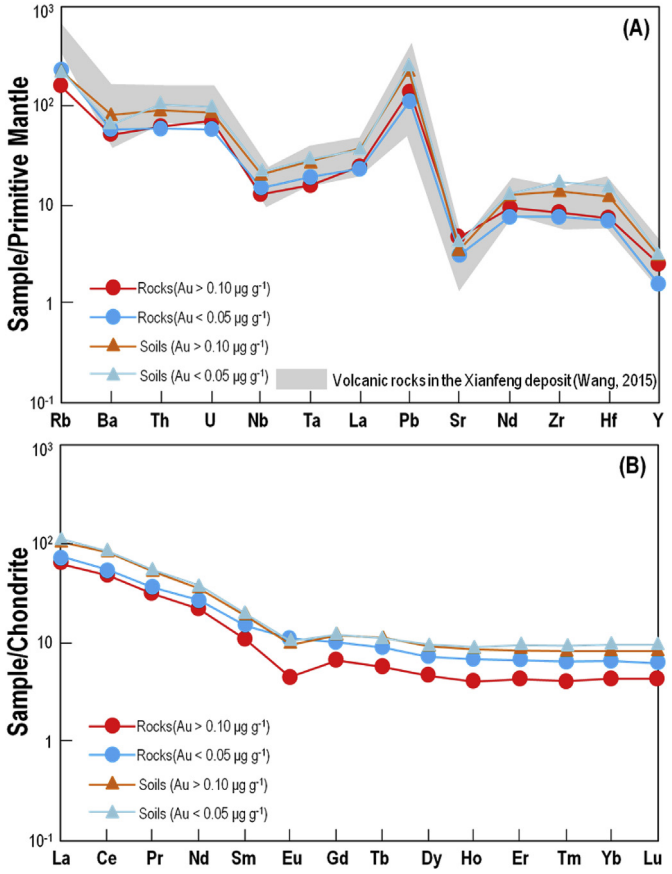

Fig. 4. **A** Primitive Mantle (PM)-normalized diagram for large ion lithophile elements and high field strength elements in rocks and soils from the Xianfeng gold deposit; **B** Chondrite-normalized diagram for REE in rocks and soils from the Xianfeng gold deposit. (For interpretation of the references to color in this figure legend, the reader is referred to the Web version of this article.)

were 91–104% (n = 3) and 95–107% (n = 3), respectively, and coefficients of variation (triplicate analyses) were within 10%.

According to the Hg concentrations measured above, 0.2 g of soil samples were digested (95 °C, 6 h) in 2 mL aqua regia ($HCl:HNO_3$ = 3:1, v:v). The digests were diluted to 0.5 ng mL^{-1} Hg with acid concentration adjusted to 10–20% (v/v), prior to Hg isotope analysis using Neptune Plus multiple collector inductively coupled plasma mass spectrometer (MC-ICP-MS), following a previous method (Yin et al., 2016b). δ^{202}Hg, Δ^{199}Hg, Δ^{200}Hg, and Δ^{201}Hg were calculated relative to NIST SRM 3133, following the recommended standard-sample-standard bracketing protocol (Blum and Bergquist, 2007). Mercury concentrations and acid matrices in the bracketing NIST SRM 3133 solutions were matched with neighboring samples. NIST SRM 2711 (n = 2) and MESS-1 (n = 2) were prepared and measured in the same way with the samples. UM-Almadén secondary solutions (0.5 ng mL^{-1} Hg) were prepared in 10% (v/v) aqua regia solutions and measured between every ten samples. Analytical accuracy and uncertainties were

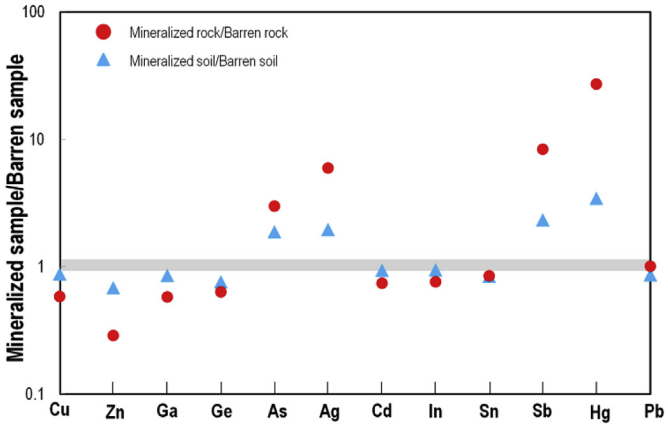

Fig. 5. Enrichments of chalcophile elements in mineralized rocks and soils from the Xianfeng gold deposit. (For interpretation of the references to color in this figure legend, the reader is referred to the Web version of this article.)

estimated based on replication of the UM-Almadén secondary standard solution (δ^{202}Hg: −0.52 ± 0.09‰; Δ^{199}Hg: −0.03 ± 0.05‰; 2SD, n = 11) and full procedural analyses of NIST SRM 2711a (δ^{202}Hg: −0.14 ± 0.13‰; Δ^{199}Hg: −0.22 ± 0.05‰; 2SD, n = 2) and MESS-1 (δ^{202}Hg: −1.89 ± 0.10‰; Δ^{199}Hg: 0.04 ± 0.04‰; 2SD, n = 2). These results are comparable with previous results (Blum and Bergquist, 2007; Biswas et al., 2008; Sherman et al., 2009; Donovan et al., 2013; Yin et al., 2016b). Analytical uncertainties reflect the larger values of standard deviation (2SD) for either UM-Almadén or SRMs.

2.4. Statistical analysis

Detailed results of gold and trace element concentrations and Hg isotopic compositions were summarized in Supplementary Tables S1, S2, S3, and S4. Data were analyzed in SPSS (version 13.0). Correlation coefficients (R) and significance probabilities (p) were computed for the linear regression fits according to Pearson correlation analysis. One-way analysis of variance (ANOVA) was carried out to compare whether concentrations and isotopic compositions varied significantly between different sample groups.

3. Results and discussion

3.1. Gold concentrations

Bulk gold concentrations in rocks and soils range from <0.05 to 5.20 μg g^{-1} (n = 54) and <0.05–0.82 μg g^{-1} (n = 43), respectively (Table S1). Except for some samples that showed gold concentrations lower than the detection limit (0.05 μg g^{-1} Au), other samples showed elevated gold concentrations of >0.10 μg g^{-1}. Following our previous protocol (Yin et al., 2019), the samples were classified into two groups according to gold concentration, i.e., samples with Au > 0.10 μg g^{-1} as mineralized samples (denoted as $rocks_{Au>0.10}$ or $soils_{Au>0.10}$), and samples with Au <0.05 μg g^{-1} as barren samples (denoted as $rocks_{Au<0.05}$ or $soils_{Au<0.05}$).

As shown in Fig. 3, $rocks_{Au>0.10}$ are located in the mineralization zones (breccias and veins), and cracks and faults played an important role in controlling the gold mineralization. Although no clear correlation ($p > 0.05$) in gold concentrations was observed between the paired rock and soil samples, it is clear that $soils_{Au>0.10}$ are located above or near the mineralization zones (Fig. 3), indicating that these soils received gold from the weathering of underlying rocks.

3.2. Large ion lithophile elements, high field strength elements, and rare earth elements

The concentrations LILE (Rb, Cs, Sr, Ba, and U, summarized in Table S1) and HFSE (Nb, Ta, Zr, Hf, Th and Ti, summarized in Table S1), and REE (La, Ce, Pr, Nd, Sm, Eu, Gd, Tb, Dy, Ho, Er, Tm, Yb and Lu, summarized in Table S2) displayed log-normal distributions, therefore their geometric mean values were calculated. The geometric mean concentrations of LILE for rock and soil samples were plotted in the Primitive Mantle (PM)-normalized diagram (Fig. 4A). It can be seen that both mineralized $rocks_{Au>0.10}$ and barren $rocks_{Au<0.05}$ show consistent patterns. A similar pattern (Fig. 4A), which reflects a subduction-related tectonic setting (e.g., convergent margin and volcanic arc), has been previously reported for magmatic rocks in the studied area (Wang, 2015). Studies have demonstrated that subduction of the Paleo-Pacific Ocean in the Early Cretaceous generated large volumes of magmatic rocks, which have close spatiotemporal relations to the hydrothermal gold mineralization in NE China (Wu et al., 2011; Xu et al., 2013; Hao et al., 2016; Zhi et al., 2016). The geometric mean

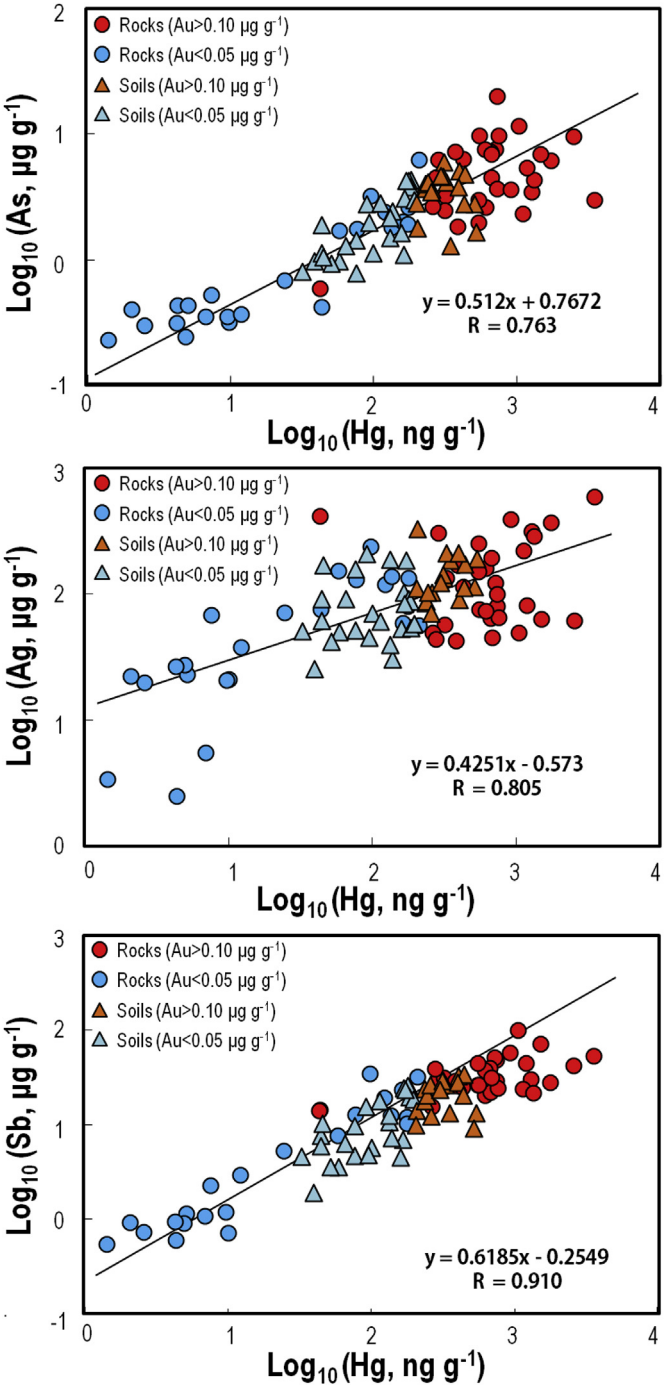

Fig. 6. Correlations between As and Hg, Ag, and Hg, and Sb and Hg in rocks and soils from the Xianfeng gold deposit. (For interpretation of the references to color in this figure legend, the reader is referred to the Web version of this article.)

concentrations of REE in rock and soil samples are presented in the Chondrite-normalized REE diagram (Fig. 4B). It can be seen that both the mineralized $rocks_{Au>0.10}$ and barren $rocks_{Au<0.05}$ show similar REE distribution patterns, with negative Eu anomalies. Negative Eu anomalies were also reported for Early Cretaceous felsic igneous rocks in NE China, where magma originated from the melting of the lower crust (Xu et al., 2013).

As shown in Fig. 4A and B, $soils_{Au>0.10}$ and $soils_{Au<0.05}$ all show very similar PM-normalized HFSE-LILE patterns and REE distribution patterns with the underlying rocks, suggesting that the

weathered horizon over the Xianfeng deposit was well-preserved in spite of subsequent leaching, seepage, and solid physical processes. LILE and HFSE, and REE are immobile elements, therefore they remain as the residual phase in the weathered horizon (Middelburg et al., 1988; Maulana et al., 2014). This can be proven by the slightly elevated contents of LILE and HFSE, and REE in soils, compared to the parent rocks (Fig. 4A and B).

3.3. Chalcophile elements

The concentrations of chalcophile elements (Cu, Zn, Ga, Ge, As, Ag, Cd, In, Sn, Sb, Tl, and Pb, summarized in Table S3) also showed a log-normal distribution. To understand the enrichment of chalcophile elements in the Xianfeng deposits, their geometric mean concentrations in $rocks_{Au>0.10}$, $rocks_{Au<0.05}$, $soils_{Au>0.10}$ and $soils_{Au<0.05}$ are calculated individually, and the concentration ratios for $rocks_{Au>0.10}/rocks_{Au<0.05}$ and $soils_{Au>0.10}/soils_{Au<0.05}$ were estimated. As shown in Fig. 5, positive $rocks_{Au>0.10}/rocks_{Au<0.05}$ ratios of 3–30 were observed for As, Ag, Sb and Hg, suggesting the enrichment of these metals in mineralized $rocks_{Au>0.10}$. Positive $soils_{Au>0.10}/soils_{Au<0.05}$ ratios of 2–4 were also observed for As, Ag, Sb, and Hg. Considering As, Ag, Sb and Hg are toxic heavy metals, the enrichment of these metals in the $rocks_{Au>0.10}$ and $soils_{Au>0.10}$ is of great environmental concern. The enrichment of element suite Ag–As–Sb–Hg in the Xianfeng deposit is consistent with the general features of hydrothermal gold deposits (Hedenquist et al., 2000; Saunders et al., 2014). The element suite Ag–As–Sb–Hg was thought to be concentrated in active hydrothermal systems at the final low-temperature stages (Simmons et al., 2005).

We assessed the relationships between As, Ag, and Sb against Hg concentration in all rock and soil samples given that Hg demonstrates one of the strongest bonds with sulfide-containing minerals. As shown in Fig. 6, As, Ag and Sb display significantly positive correlations with Hg in all rock and soil samples (R^2 = *0.763 to 0.910*, $p < 0.05$), suggesting that the enrichment of Ag–As–Sb–Hg took place synchronously. As shown in Fig. 7, significantly positive correlations in As, Ag, Sb and Hg concentrations (R^2 = *0.539 to 0.782*; $p < 0.05$) were observed between paired rock and soil samples, indicating that the weathering of the epithermal gold orebodies resulted in the release and fixation of large amounts of As, Ag, Sb, and Hg in the weathered horizon. The Ag–As–Sb–Hg anomalies in the weathered horizon are of environmental concern but can be used as indicators for prospecting shallowly buried epithermal gold orebodies.

3.4. Mercury isotopic composition

According to our recent study (Yin et al., 2019), no significant differences ($p > 0.05$, ANOVA) in Hg isotopic compositions and particularly in the MIF (Δ^{199}Hg) were observed between mineralized $rocks_{Au>0.10}$ (δ^{202}Hg: −0.23 ± 0.72‰; Δ^{199}Hg: −0.02 ± 0.12‰; 2SD, n = 33) and barren $rocks_{Au<0.05}$ (δ^{202}Hg: −0.45 ± 0.44‰; Δ^{199}Hg: −0.01 ± 0.12‰; 2SD, n = 13). Similar Hg isotopic compositions have been reported in igneous rocks in the California Coast Ranges, USA (δ^{202}Hg: −0.6 ± 0.5‰; Δ^{199}Hg: 0 ± 0.2‰) (Smith et al., 2008). Little to no Hg-MDF (<±0.5‰ in δ^{202}Hg) and Hg-MIF occur during the leaching of Hg from source rocks (Smith et al., 2008), suggests that Hg in the Xianfeng gold deposit is mainly derived from magmatic rocks.

We compared Hg isotopic compositions between soil and rock samples. The mineralized $soils_{Au>0.10}$ (δ^{202}Hg: −0.44 ± 0.60‰; Δ^{199}Hg: −0.03 ± 0.14‰; 2SD, n = 15) and barren $soils_{Au<0.05}$ (δ^{202}Hg: −0.54 ± 0.68‰; Δ^{199}Hg: −0.05 ± 0.14‰; 2SD, n = 28) showed similar Hg isotopic composition to the rock samples. As shown in Fig. 8, soils and rocks from the Xianfeng gold deposits are isotopically overlapped, indicating that all samples analyzed originated from the hydrothermal system, including those marked as barren samples with respect to their Au content. This is due to the much larger dispersion halo of Hg compared to Au (Yin et al., 2019).

Previous studies reported the isotopic signature of Hg in organic

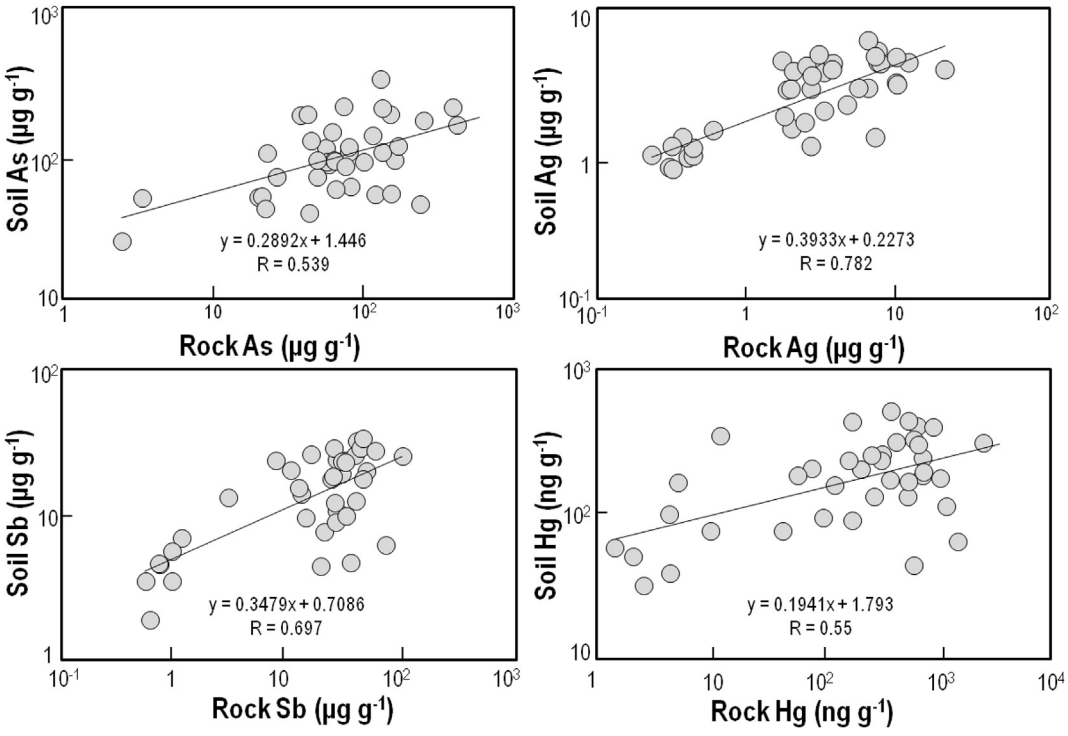

Fig. 7. Correlations in As, Ag, Sb and Hg concentrations between the paired rock and soil samples from the Xianfeng gold deposit.

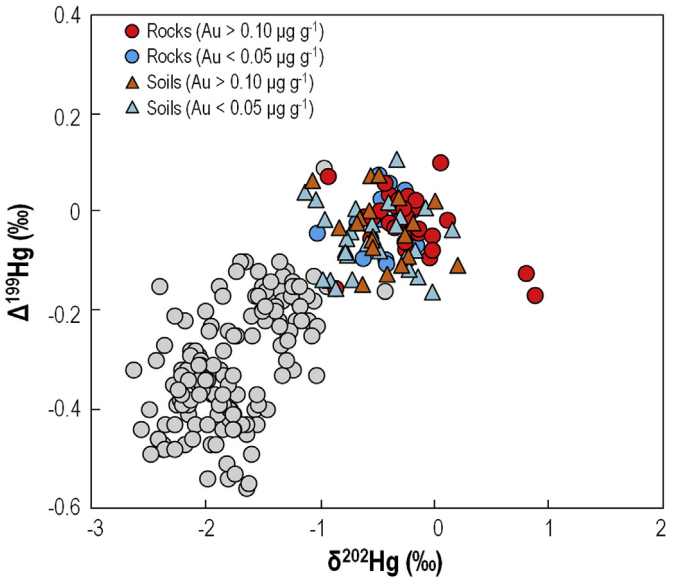

Fig. 8. Mercury isotopic composition of rocks and soils from the Xianfeng gold deposit., and surface soils from pristine areas (Biswas et al., 2008; Demers et al., 2013; Zhang et al., 2013; Zheng et al., 2016; Wang et al., 2016; Jiskra et al., 2017). (For interpretation of the references to color in this figure legend, the reader is referred to the Web version of this article.)

soils collected from pristine areas and suggested that organic soil mainly receive Hg from atmospheric deposition (Biswas et al., 2008; Demers et al., 2013; Zhang et al., 2013; Obrist et al., 2017; Zheng et al., 2016; Wang et al., 2016). As shown in Fig. 8, surface soils collected from pristine areas were characterized by negative δ^{202}Hg and Δ^{199}Hg, which are significantly distinct from soils from this study. Regarding horizon B, the magnitude of atmospheric Hg deposition relative to the direct weathering influence is also likely much smaller. This suggests a limited contribution of atmospheric Hg deposition in the weathered horizon over the Xianfeng gold deposit. As mentioned earlier, weathering of rocks is the major mechanism for the Hg enrichment in the Xianfeng soils. Although recent studies demonstrated that significant MDF of Hg isotopes could occur during Hg(II) reduction, Hg(II) adsorption, Hg (0) volatilization and leaching processes (Blum et al., 2014), it seems that these processes may not significantly alter the isotopic signature of Hg in the weathered horizon because only a small fraction of Hg is lost compared to the soil Hg pool. The lack of significant Hg isotope fractionation in the weathered horizon may be supported by recent studies on soils from mining areas (Sonke et al., 2010; Donovan et al., 2013; Yin et al., 2013a; Yin et al., 2013b; Gray et al., 2013). Contaminated soils from mining areas (δ^{202}Hg: -0.5 ± 0.8‰; Δ^{199}Hg: 0.0 ± 0.2‰, 2SD) showed consistent Hg isotope signatures to ore minerals, indicating Hg isotopes in soils (especially mineral soils) are less altered by weathering as well as various geochemical processes. All in all, we suggest that the measurements of Hg isotopes in rocks and soils in naturally Hg-contaminated regions can help identify locations of epithermal gold deposits.

4. Conclusions and implications

Through investigation of trace metals concentrations, and Hg isotopic composition, conclusions can be summarized: (1) Consistent distribution patterns in soils and rocks were observed for immobile elements of the HFSE, LILE and REE family, reflecting the subduction-related tectonic setting; (2) Hydrothermal processes have resulted in synchronous enrichment of As, Ag, Sb, and Hg in gold orebodies, and weathering of orebodies releases large amounts of As, Ag, Sb, and Hg to the weathered horizon; (3) Hg isotopes further confirm that Hg in the weathered horizon is derived from the underlying rocks, and limited Hg isotope fractionation seems to occur during the formation of weathered horizon. The consistent geochemical patterns between rocks and weathered horizon reveal evidence of a simple and direct geochemical link between this shallow buried hydrothermal deposit and its weathered horizon. Combine the As–Ag–Sb–Hg anomalies in the B horizon soil, with further Hg isotope tracing that demonstrate Hg is originated from underlying deposits, the use of soil geochemistry surveys can be an effective tool in prospecting of shallowly buried epithermal gold deposits. Hydrothermal deposits contain abundant heavy metals (e.g., Hg, As and Sb). This study also implies that weathering processes the shallow buried hydrothermal deposits may facilitate the release of these heavy metals to surface soil and caused environmental concerns.

CRediT authorship contribution statement

Runsheng Yin: Conceptualization, Methodology, Writing - original draft. **Xin Pan:** Validation, Formal analysis. **Changzhou Deng:** Validation, Formal analysis. **Guangyi Sun:** Validation, Formal analysis. **Sae Yun Kwon:** Writing - review & editing. **Ryan F. Lepak:** Writing - review & editing. **James P. Hurley:** Writing - review & editing.

Acknowledgments

Guanghui Li, Yongwei Huang, and Enbao Wang are acknowledged for their aid with field sampling. USGS Wisconsin Mercury Research Lab and Wisconsin State Lab of Hygiene are thanked for the use of their lab facilities for stable Hg isotope determination. Professor Bernd Lehmann from the Technical University of Clausthal is thanked for giving thoughtful comments. This work was supported by the National Natural Science Foundation of China (41873047, 41603020). Three anonymous reviewers were acknowledged for their constructive comments that have largely improved the quality of this paper.

Appendix A. Supplementary data

Supplementary data to this article can be found online at https://doi.org/10.1016/j.envpol.2020.113954.

References

Bergquist, B.A., Blum, J.D., 2009. The odds and evens of mercury isotopes: applications of mass-dependent and mass-independent isotope fractionation. Elements 5 (6), 353–357.
Biswas, A., Blum, J.D., Bergquist, B.A., Keeler, G.J., Xie, Z., 2008. Natural mercury isotope variation in coal deposits and organic soils. Environ. Sci. Technol. 42 (22), 8303–8309.
Bradshaw, P.M.D., Thomson, I., Hood, P.J., 1979. The application of soil sampling to geochemical exploration in nonglaciated regions of the world. In Geophysics and Geochemistry in the Search for Metallic Ores. Geol. Surv. Can. 31, 327–338.
Blum, J.D., Bergquist, B.A., 2007. Reporting of variations in the natural isotopic composition of mercury. Anal. Bioanal. Chem. 388, 353–359.
Blum, J.D., Sherman, L.S., Johnson, M.W., 2014. Mercury isotopes in earth and environmental sciences. Annu. Rev. Earth Planet Sci. 42, 249–269.
Demers, J.D., Blum, J.D., Zak, D.R., 2013. Mercury isotopes in a forested ecosystem: implications for air-surface exchange dynamics and the global mercury cycle. Glob. Biogeochem. Cycles 27 (1), 222–238.
Donovan, P.M., Blum, J.D., Yee, D., Gehrke, G.E., Singer, M.B., 2013. An isotopic record of mercury in San Francisco Bay sediment. Chem. Geol. 349, 87–98.
Freyssinet, P., Itard, Y., Gubins, A.G., 1997. Geochemical mass balance of gold under various tropical weathering conditions: application to exploration. Explorations 97, 347–354.
Gray, J.E., Pribil, M.J., Higueras, P.L., 2013. Mercury isotope fractionation during ore retorting in the Almadén mining district, Spain. Chem. Geol. 357, 150–157.

Han, S.J., Sun, J.G., Bai, L.A., Xing, S.W., Chai, P., Zhang, Y., Yang, F., Meng, L.J., Li, Y.X., 2013. Geology and ages of porphyry and medium-to high-sulphidation epithermal gold deposits of the continental margin of Northeast China. Int. Geol. Rev. 55 (3), 287–310.

Hao, B.W., Deng, J., Bagas, L., Ge, L.S., Nie, F.J., Turner, S., Qing, M., 2016. The Gaosongshan epithermal gold deposit in the lesser Hinggan range of the Heilongjiang province, NE China: implications for Early Cretaceous mineralization. Ore Geol. Rev. 73, 179–197.

Hedenquist, J.W., Arribas, Antonio, Gonzalez-Urien, E., 2000. Exploration for epithermal gold deposits. Rev. Econ. Geol. 13 (2), 45–77.

Hintelmann, H., Lu, S., 2003. High precision isotope ratio measurements of mercury isotopes in cinnabar ores using multi-collector inductively coupled plasma mass spectrometry. Analyst 128, 635–639.

Jiskra, M., Wiederhold, J.G., Skyllberg, U., Kronberg, R.M., Kretzschmar, R., 2017. Source tracing of natural organic matter bound mercury in boreal forest runoff with mercury stable isotopes. Environ. Sci.: Processes & Impacts 19 (10), 1235–1248.

Kwon, S.Y., Blum, J.D., Nadelhoffer, K.J., Dvonch, J.T., Tsui, M.T.K., 2015. Isotopic study of mercury sources and transfer between a freshwater lake and adjacent forest food web. Sci. Total Environ. 532, 220–229.

Li, G.H., 2011. Metallogenetic Series and Exploration Prediction in the Taipingling-Wandashan Menerogenetic Zone of Heilongjiang. Dissertation, China University of Geosciences (In Chinese with English abstract).

Maulana, A., Yonezu, K., Watanabe, K., 2014. Geochemistry of rare earth elements (REE) in the weathered crusts from the granitic rocks in Sulawesi Island, Indonesia. J. Earth Sci. 25 (3), 460–472.

Middelburg, J.J., van der Weijden, C.H., Woittiez, J.R.W., 1988. Chemical processes affecting the mobility of major, minor and trace elements during weathering of granitic rocks. Chem. Geol. 68 (3–4), 253–273.

Obrist, D., Agnan, Y., Jiskra, M., Olson, C.L., Colegrove, D.P., Hueber, J., 2017. Tundra uptake of atmospheric elemental mercury drives Arctic mercury pollution. Nature 547 (7662), 201–204.

Rytuba, J.J., 2003. Mercury from mineral deposits and potential environmental impact. Environ. Geol. 43, 326–338.

Saunders, J.A., Hofstra, A.H., Goldfarb, R.J., Reed, M.H., 2014. Geochemistry of hydrothermal gold deposits-13.15. Treatise geochem. 2 (3), 383–424.

Sherman, L.S., Blum, J.D., Nordstrom, D.K., McCleskey, R.B., Barkay, T., Vetriani, C., 2009. Mercury isotopic composition of hydrothermal systems in the Yellowstone Plateau volcanic field and Guaymas Basin sea-floor rift. Earth Planet. Sci. Lett. 279, 86–96.

Sholupov, S., Pogarev, S., Ryzhov, V., Mashyanov, N., Stroganov, A., 2004. Zeeman atomic absorption spectrometer RA-915+ for direct determination of mercury in air and complex matrix samples. Fuel Process. Technol. 85 (6), 473–485.

Simmons, S.F., White, N., John, D.A., 2005. Geological characteristics of epithermal precious and base metal deposits. Econ. Geol. One Hundredth Anniv. Vol. 485–522.

Smith, C.N., Kesler, S.E., Blum, J.D., Rytuba, J.J., 2008. Isotope geochemistry of mercury in source rocks, mineral deposits and spring deposits of the California Coast Ranges, USA. Earth Planet. Sci. Lett. 269, 399–407.

Smith, C.N., Kesler, S.E., Klaue, B., Blum, J.D., 2005. Mercury isotope fractionation in fossil hydrothermal systems. Geology 33, 825.

Sonke, J.E., Schäfer, J., Chmeleff, J., Audry, S., Blanc, G., Dupré, B., 2010. Sedimentary mercury stable isotope records of atmospheric and riverine pollution from two major European heavy metal refineries. Chem. Geol. 279, 90–100.

Sonke, J.E., 2011. A global model of mass independent mercury stable isotope fractionation. Geochem. Cosmochim. Acta 75 (16), 4577–4590.

Sun, M.D., Xu, Y.G., Wilde, S.A., Chen, H.L., Yang, S.F., 2015. The permian dongfanghong island-arc gabbro of the wandashan orogen, NE China: implications for paleo-pacific subduction. Tectonophysics 659, 122–136.

Tan, Q.P., Xia, Y., Xie, Z.J., Yan, J., 2015. Migration paths and precipitation mechanisms of ore-forming fluids at the Shuiyindong Carlin-type gold deposit, Guizhou, China. Ore Geol. Rev. 69, 140–156.

Tang, Y., Bi, X., Yin, R., Feng, X., Hu, R., 2017. Concentrations and isotopic variability of mercury in sulfide minerals from the Jinding Zn-Pb deposit, Southwest China. Ore Geol. Rev. 90, 958–969.

Wang, Q.S., 2015. Geological Characteristics and Genesis of the Xianfengbeishan Gold Deposit in Wandashan Area, Heilongjiang Province. Dissertation, Jilin university (in Chinese with English abstract).

Wang, X., Luo, J., Yin, R., Yuan, W., Lin, C.J., Sommar, J., 2016. Using mercury isotopes to understand mercury accumulation in the montane forest floor of the eastern Tibetan plateau. Environ. Sci. Technol. 51 (2), 801–809.

Wu, F.Y., Sun, D.Y., Ge, W.C., Zhang, Y.B., Grant, M.L., Wilde, S.A., Jahn, B.M., 2011. Geochronology of the Phanerozoic granitoids in northeastern China. J. Asian Earth Sci. 41, 1–30.

Wu, F.Y., Zhao, G.C., Sun, D.Y., Wilde, S.A., Yang, J.H., 2007. The hulan group: its role in the evolution of the central asian orogenic Belt of NE China. J. Asian Earth Sci. 30, 542–556.

Xu, C., Yin, R., Peng, J., Hurley, J.P., Lepak, R.F., Gao, J., Feng, X., Hu, R., Bi, X., 2017. Mercury isotope constraints on the source for sediment-hosted lead-zinc deposits in the Changdu area, southwestern China. Miner. Depos. 53 (3), 339–352.

Xu, W.L., Pei, F.P., Wang, F., Meng, E., Ji, W.Q., Yang, D.B., Wei, W., 2013. Spatial-temporal relationships of Mesozoic volcanic rocks in NE China: constraints on tectonic overprinting and transformations between multiple tectonic regimes. J. Asian Earth Sci. 74, 167–193.

Yin, R., Feng, X., Hurley, J.P., Krabbenhoft, D.P., Lepak, R.F., Hu, R., 2016a. Mercury isotopes as proxies to identify sources and environmental impacts of mercury in sphalerites. Sci. Rep. 6, 18686.

Yin, R., Krabbenhoft, D.P., Bergquist, B.A., Zheng, W., Lepak, R.F., Hurley, J.P., 2016b. Effects of mercury and thallium concentrations on high precision determination of mercury isotopic composition by Neptune Plus multiple collector inductively coupled plasma mass spectrometry. J. Anal. At. Spectrom. 31 (10), 2060–2068.

Yin, R., Feng, X., Wang, J., Bao, Z., Yu, B., Chen, J., 2013b. Mercury isotope variations between bioavailable mercury fractions and total mercury in mercury contaminated soil in Wanshan Mercury Mine, SW China. Chem. Geol. 336, 80–86.

Yin, R., Feng, X., Wang, J., Li, P., Liu, J., Zhang, Y., Zheng, L., Hu, T., 2013a. Mercury speciation and mercury isotope fractionation during ore roasting process and their implication to source identification of downstream sediment in the Wanshan mercury mining area, SW China. Chem. Geol. 336, 72–79.

Yin, R., Deng, C., Lehmann, B., Sun, G., Lepak, R.F., Hurley, J.P., Zhao, C., Xu, G., Tan, Q., Xie, Z., Hu, R., 2019. Magmatic-hydrothermal origin of mercury in Carlin-style and epithermal gold deposits in China: evidence from mercury stable isotopes. ACS Earth Space Chem. 2019. https://doi.org/10.1021/acsearthspacechem.9b00111.

Zhai, D., Liu, J., Ripley, E.M., Wang, J., 2015. Geochronological and He–Ar–S isotopic constraints on the origin of the Sandaowanzi gold-telluride deposit, northeastern China. Lithos 212, 338–352.

Zhang, H., Yin, R.S., Feng, X.B., Sommar, J., Anderson, C.W., Sapkota, A., Fu, X., Larrsen, T., 2013. Atmospheric mercury inputs in montane soils increase with elevation: evidence from mercury isotope signatures. Sci. Rep. 3, 3322.

Zheng, W., Obrist, D., Weis, D., Bergquist, B.A., 2016. Mercury isotope compositions across North American forests. Glob. Biogeochem. Cycles 30 (10), 1475–1492.

Zhou, T., Goldfarb, R.J., Phillips, N.G., 2002. Tectonics and distribution of gold deposits in China–an overview. Miner. Depos. 37 (3–4), 249–282.

Zhi, Y.B., Li, B.L., Xi, A.H., Xu, Q.L., Zhang, L., Sun, Y.G., Chang, J.J., Peng, B., 2016. Geochronology and geochemistry of the major host rock of the Dong'an gold deposit, Lesser Khingan range: implication for petrogenesis and metallogenic setting during the Early-middle Jurassic in northeast China. Chem. Erde 76, 257–274.